Author Manuscript

Title: Deinterpenetration of IRMOF-9

Authors: Audrey B. Crom; Joseph L. Strozier; Caleb J. Tatebe; Cassidy A. Carey; Jeremy I. Feldblyum; Douglas Genna

This is the author manuscript accepted for publication. It has not been through the copyediting, typesetting, pagination and proofreading process, which may lead to differences between this version and the Version of Record.

To be cited as: 10.1002/chem.202302856

Link to VoR: https://doi.org/10.1002/chem.202302856

Communication

Deinterpenetration of IRMOF-9

Audrey B. Crom,[b] Joseph L. Strozier,[a] Caleb J. Tatebe,[a] Cassidy A. Carey,[c] Jeremy I. Feldblyum,*[b] Douglas T. Genna*[a]

[a] J. L. Strozier, C. J. Tatebe, Prof. D. T. Genna
Department of Chemistry WBSH5053
Youngstown State University
Youngstown, OH 44555
E-mail: dtgenna@ysu.edu

[b] A. B. Crom, Prof. J. I. Feldblyum
Department of Chemistry
University at Albany, State University of New York
Albany, NY 12222
Email: jfeldblyum@albany.edu

[c] C. A. Carey
Department of Chemistry
University of Michigan
Ann Arbor, MI 48105

Supporting information for this article is given via a link at the end of the document.((Please delete this text if not appropriate))

Abstract: One of the iconic characteristics of metal–organic frameworks (MOFs) is the possesssion of guest-accessible pores. Increasing pore size has a direct and often beneficial impact on a MOF's adsorption and separation properties. However, as pore size increases, the resulting void spaces are often filled by interpenetrated frameworks, where one or more networks crystallize within the pore system of another identical network, reducing the MOF's free volume and pore size. Furthermore, due to the thermodynamic favorability of interpenetration during solvothermal synthesis, techniques to synthetically differentiate interpenetrated from non-interpenetrated MOFs are paramount. Herein we report the synthesis of deinterpenetrated IRMOF-9 *via* halide mediated deinterpenetrative conversion of Zn_4O-derived IRMOF-9. IRMOF-9, when treated with ethylammonium bromide, is quasi-selectively etched, revealing the non-interpenetrated analogue, IRMOF-10 (deinterpenetrated IRMOF-9), which can be isolated prior to complete dissolution by the bromide solution. Dye adsorption, surface area and pore size distribution analysis, and powder X-ray diffraction are consistent with successful deinterpenetration.

Metal–organic frameworks (MOFs)[1] have become gradually more popular due to their promising potential in applications such as molecular storage/separations,[2] catalysis,[3] drug delivery,[4] etc.[5] As demands for greater storage capacity increased, the race to systematically synthesize larger and larger pore volumes began in earnest with the IRMOF (isoreticular MOF) series.[6] However, as the pore sizes and void volumes increased, it became possible for additional frameworks to grow within these voids. The resulting materials, known as interpenetrated MOFs[7] maximized packing efficiency while simultaneously decreasing guest storage capacities and available pore volume.[8]

In most cases, the interpenetrated isomer of a MOF is thermodynamically favored.[8a] In order to control the outcome of a given MOF synthesis and directly yield the non-interpenetrated framework,[9] solvothermal synthesis under significant dilution (when compared to their interpenetrated counterparts) is generally necessary.[10] However, this approach leads to large amounts of waste, low yields, and often phase-impure material.

Previously, our group reported the halide-mediated penetration of the $[In(CO_2R)_4]^-$-derived 3-dimensional MOF ATF-1 to the non-interpenetrated 2-dimensional isomer YCM-21.[11] This transformation is proposed to proceed through the temporary formation of an $[In(CO_2R)_3X]^-$ (X = halide) inorganic-node formed by the reaction of the $[In(CO_2R)_4]^-$ with exogenous halide. This halogenated intermediate allows for the interpenetrated frameworks to "unhook" from each other, prior to reformation of the $[In(CO_2R)_4]^-$ center. Once this unhooking mechanism occurs across the totality of the MOF, two independent frameworks are formed.

We hypothesized that a similar strategy could be employed with MOFs containing the $Zn_4O(CO_2R)_6$ cluster commonly found in the IRMOF series, thus allowing for the synthesis of deinterpenetrated IRMOFs from their interpenetrated counterparts. Herein we report the successful deinterpenetration of IRMOF-9.

The IRMOF-9/IRMOF-10 isomeric pair derived from the Zn_4O-cluster and 4,4'-biphenyldicarboxylic acid (H_2BPDC) has been studied extensively[10b, 12] since its original report by Yaghi.[6] Phase pure synthesis of IRMOF-10 has been difficult to achieve and characterize.

When we applied our optimized conditions for deinterpenetration, which were previously developed for the conversion of ATF-1 to YCM-21[11] (0.16 M solution of Et_4NBr in DMF:CH_2Cl_2 (1:1 v:v) at 120 °C), for the deinterpenetration of IRMOF-9 (synthesized using the protocol from Rowsell and Yaghi[12a]), the MOF visibly displayed signs of dissolution after 24 hours. However, when IRMOF-9 was subjected to the same reaction solution at room temperature instead of 120 °C (Figure 1), no dissolution was observed. Analysis with both PXRD (Figure S1) and optical microscopy (Figure S2) indicated that the crystalline structure was intact albeit diminished after 2 days. However, due to the stress induced on the framework during conversion, the crystal quality of the product was not sufficient to

Author Manuscript

This article is protected by copyright. All rights reserved

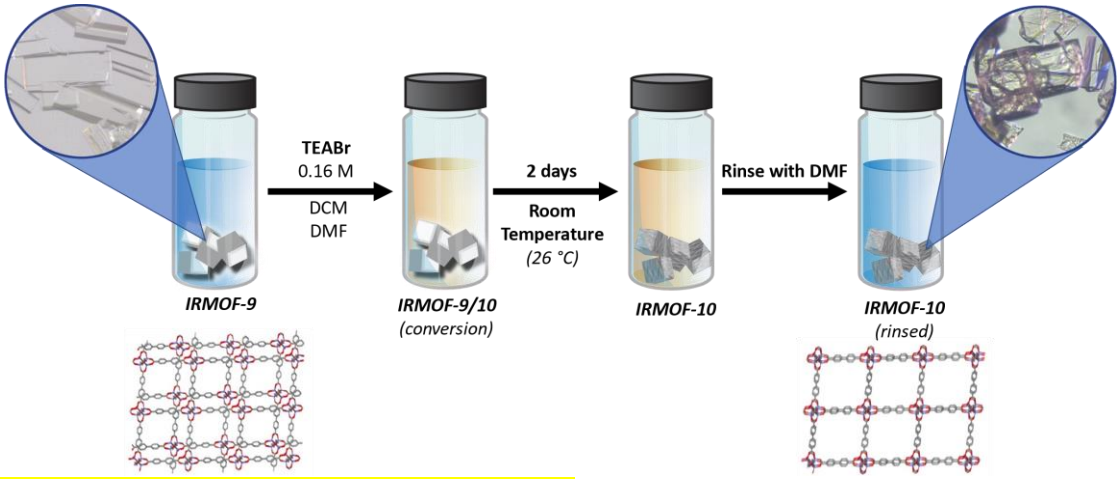


Figure 1: Synthesis of IRMOF-10 by deinterpenetrative conversion of IRMOF-9.

obtain a crystallographic model from single-crystal X-ray diffraction. Furthermore, attempts to obtain IRMOF-10 directly with a one-pot solvothermal synthesis using $Zn(NO_3)_2$, H_2BPDC, and Et_4NBr yielded neither IRMOF-10 nor IRMOF-9, regardless of the conditions tested.

UV-vis analysis of the deinterpenetrative conversion reaction solution indicated the presence of BPDC (Figure S3). ^1H NMR of the mother liquor of the reaction revealed the presence of BPDC as well (Figure S4). Additionally, after 5 h, the MOF was filtered from the deinterpenetration solution and that solution was placed in a 100 °C oven for 24 hours (the conditions necessary to grow IRMOF-9/10). Analysis after heating revealed the presence of inorganic Zn, which precipitated from solution as confirmed by PXRD analysis (Figure S5).

The presence of both BPDC and Zn^{2+} in the deinterpenetration reaction solution supports the contention that IRMOF-9 is being altered *via* partial dissolution. This can involve either (1) preferential dissolution of just one of the framework nets, leading to deinterpenetrated IRMOF-9 (IRMOF-10) or (2) indiscriminate dissolution across both frameworks yielding a material that resembles IRMOF-9 with pockets of hierarchical mesoporosity. These dissolution pathways were distinguished from each other using N_2 gas sorption analysis and dye uptake exclusion experiments.

As no single crystal structure of unfunctionalized IRMOF-10 has been reported in the literature, the synthesis of IRMOF-10 is often confirmed by comparison with the calculated powder X-ray diffraction (PXRD) pattern of IRMOF-12.[13] However, both IRMOF-9 and IRMOF-12 share many common peaks in their respective PXRD patterns (notably at 5°, 7.3°, 10.3°, and 11.6° 2θ; Figure S6). Additionally, the calculated PXRD patterns for IRMOF-9 and IRMOF-10 are nearly identical (whether by simulating IRMOF-10 as cubic by modifying IRMOF-12 or as triclinic by manually de-interpenetrating IRMOF-9), rendering their differentiation challenging (Figure S6).

Since it is challenging to rely solely on PXRD analysis to differentiate between IRMOF-9 and IRMOF-10, both pore size distribution (PSD) calculations and surface area measurements were used to distinguish the two MOFs. PSD analysis on both IRMOF-9 and its deinterpenetrated counterpart were initially carried out using density functional theory (DFT) to model experimental isotherms. PSD analysis of IRMOF-9 (Figures 2c and S7) revealed the presence of two pores, with the overwhelming majority having a diameter of 9.9 Å and a minority of pores of 11.3 Å. Deinterpenetrated IRMOF-9, which was synthesized *via* de-interpenetrative conversion, exhibited two pore sizes with the majority having a diameter of 14.9 Å and a small minority of 12.7 Å (Figures 2d and S8). The observed diameters of the major pores of both IRMOF-9 and its deinterpenetrated counterpart (9.9 Å and 14.9 Å respectively) are consistent with the expected values for the MOFs as previously determined from theoretical structures of both IRMOF-9 and IRMOF-10.[6] These findings are consistent with the formation of an IRMOF-10-like material, as opposed to an IRMOF-9 framework etched with meso/macropores (a "Swiss cheese" model). IRMOF-9 with hierarchical mesoporosity would exhibit a broad pore size distribution including pores larger than 14.9 Å while still possessing the smaller 9.9 Å and 11.3 Å pores of IRMOF-9 (attributable to the remaining portion of the still-interpenetrated framework).

Analysis of the N_2 isotherms of IRMOF-9 and its deinterpenetrated counterpart (both activated from dichloromethane) revealed BET surface areas of 1168 m^2/g and 412 m^2/g, respectively (Figures 2a and 2b, S9 and S10). It is worth noting that the N_2 isotherm of IRMOF-9 displays a two-step adsorption followed by significant hysteresis in the desorption curve in the 0-0.4 P/P_0 pressure range. This unusual behavior is indicative of structural changes leading to pore expansion (i.e., gating behavior), as previously reported during N_2 and CO_2 adsorption by Doonan and coworkers.[13] Canossa and Bacchi have reported the solvent-induced breathing/flexibility behavior of IRMOF-9 (as solved by single crystal X-ray diffraction using synchrotron irradiation) in the presence of DMF, 2-propanol, and CH_2Cl_2.[14] Furthermore, the shape of the isotherm matches that previously observed for flexible interpenetrated frameworks;[15] in contrast, the isotherm for deinterpenetrated IRMOF-9 does not exhibit this low-pressure hysteresis, nor does it possess any discernable steps. As unselective etching would not change the micropore size or dynamic behavior of the remaining material, the increased micropore size and lack of low-pressure hysteresis of the post-etched material point to conversion to IRMOF-10, rather than a simple introduction of meso- and/or macropore defects into IRMOF-9.

Our deinterpenetrated IRMOF-9 does exhibit a degree of pore collapse during activation prior to the collection of N_2

Author Manuscript

This article is protected by copyright. All rights reserved

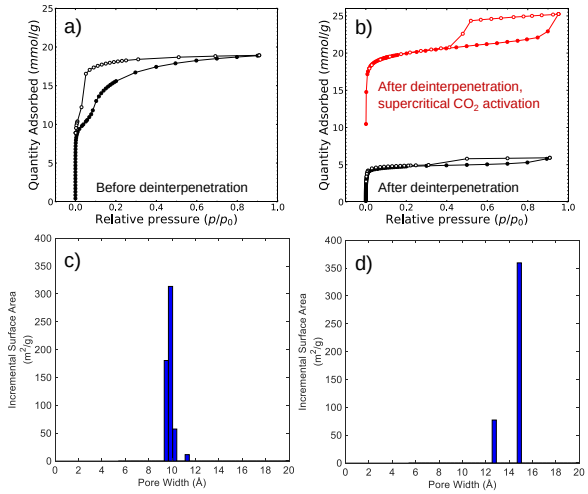


Figure 2: a) N_2 sorption isotherm of IRMOF-9 activated at room temperature and reduced pressure (~200 mTorr) for 48 hours. b) N_2 sorption isotherm of deinterpenetrated IRMOF-9 activated at room temperature and reduced pressure (~200 mTorr) for 24 hours (black trace) or with flowing supercritical CO_2 (red trace; ●, adsorption; ○, desorption). c) Pore diameter distribution for IRMOF-9 based on a DFT fit. The majority pore diameter is 9.9 Å. d) Pore diameter distribution for deinterpenetrated IRMOF-9 based on DFT fit. The majority pore-diameter is 14.9 Å.

isotherm data (see Figure S11 for PXRD patterns before and after activation). Large pore zinc MOFs, e.g., Zn-BPDC MOFs, have been shown to undergo pore collapse under even low mechanical stress, such as that which the MOF would be exposed to under conventional reduced pressure activation conditions.[16] Rapid desolvation has been shown to result in structural collapse of large-pore Zn_4O MOFs due to a slip of the {100} layers in the <001> direction.[17]

To reduce the extent of pore collapse, the deinterpenetrated sample was activated with flowing supercritical CO_2.[18] Analysis by N_2 gas sorption revealed a BET surface area of 1778 m^2/g substantially higher than that achieved both with the parent IRMOF-9 and with the deinterpenetrated sample activated under reduced pressure. X-ray diffraction after activation shows broader reflections suggestive of some loss of crystalline order, but well-matched to those expected for IRMOF-10 (Figure S12) and better defined than those observed after activation under reduced pressure (Figure S11). These data are consistent with successful deinterpenetration of IRMOF-9.

Given some loss in crystallinity during activation, the structural integrity of the pores of deinterpenetrated IRMOF-9 prior to activation was established by size exclusion dye uptake experiments. As previously reported by Yaghi,[6] IRMOF-9 has an accessible pore aperture of 10.6 Å while IRMOF-10 has an accessible pore aperture of 15.4 Å. However, we conducted our own assessment of the pore size apertures of both IRMOF-9 and IRMOF-10 using PoreBlazer.[19] These simulations revealed that the apertures are smaller than originally reported, with IRMOF-9 having a pore aperture of only 8.1 Å and IRMOF-10 having an aperture of 11.7 Å. Treatment of IRMOF-10 with a solution of Reichardt's dye (kinetic diameter ~ 11 Å) should lead to dyed crystals, while treatment of IRMOF-9 with the same dye solution should yield colorless crystals. Thus, IRMOF-9 was deinterpenetrated in the presence of Reichardt's dye, and the conversion was monitored *in situ* and confirmed *via* dye uptake. First, IRMOF-9 was immersed in a solution of 0.16 M Et_4NBr in a 1:1 DMF:DCM solution in the presence of 10 mM Reichardt's dye. The reaction was then monitored at regular time intervals by washing the crystals with fresh DCM and analyzing extent of dye uptake *via* optical microscopy (Figure 3). This *in situ* dye uptake study revealed that deinterpenetration occurs after 2 days at room temperature. After this time, the MOF crystals exhibited a blue color throughout, indicating the successful uptake of Reichardt's dye and deinterpenetration of IRMOF-9.

Uptake into the MOF's interior can be distinguished from dye adsorption to the exterior MOF surface by examining the cross-sections of these MOFs *via* optical microscopy. Cross-section analysis of the *in situ* deinterpenetrated IRMOF-9

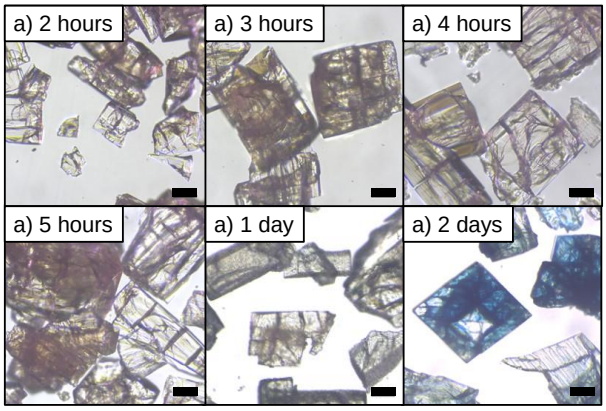


Figure 3: Optical microscope images of the *in situ* deinterpenetration of IRMOF-9 in the presence of Reichardt's dye. The indicated time points refer to the duration of exposure to the Et_4NBr-containing conversion solution. a) 2 hours, b) 3 hours, c) 4 hours, d) 5 hours, e) 1 day, and f) 2 days. Scale bar: 50 µm.

indicated that the dye was persistent throughout the crystal. Importantly, when as-synthesized IRMOF-9 was subjected to 10 mM Reichardt's dye in DMF, cross-sectional analysis confirmed no dye was incorporated within the crystal (Figure S13). We note also that when both IRMOF-9 and it's deinterpenetrated counterpart are independently treated with a saturated solution of ferrocene (kinetic diameter ~ 4 Å) in DMF, both crystals turn yellow, demonstrating that both are porous prior to and after treatment with Et_4NBr (Figures S14). These data strongly support that IRMOF-9 was deinterpenetrated *via* treatment with the Et_4NBr solution.

To assess the possibility that dye inclusion could be attributed to the accumulation of mesopore and/or macropore surface defects during exposure to the Et_4NBr solution, the infiltration of cadmium selenide quantum dots (CdSe QDs) was attempted. CdSe QDs of ca. 2 nm diameter were synthesized according to a previously reported method.[20] Deinterpenetrated IRMOF-9 was then immersed in a suspension of these QDs in DCM for 12 hours and subsequently washed in DCM before being analyzed *via* optical microscopy under UV light (Figure S15). While CdSe QDs were adsorbed to the MOF surface, penetration into the MOF interior was not observed. This observation contradicts the possibility that the successful infiltration of Reichardt's dye is attributable to meso/macroscopic defects from non-selective etching during the conversion process. Rather, these observations (lack of QD uptake, but successful small molecule dye uptake) are consistent with a successful deinterpenetration process that reveals larger pores of uniform diameter *via* the selective removal of an interpenetrating framework.

Author Manuscript

This article is protected by copyright. All rights reserved

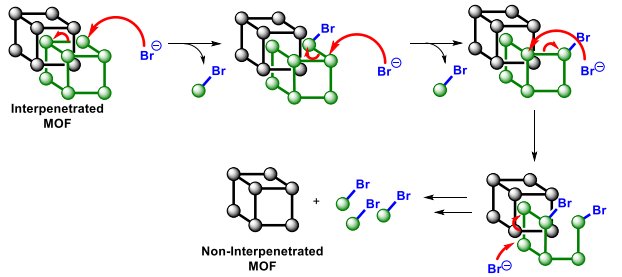


Figure 4: Cartoon of proposed mechanism of deinterpenetration. Note that curved arrows are a visual guide only and are not meant to fully represent the movement of electrons.

The pore size distribution data, lack of low-pressure hysteresis in the gas sorption isotherm, increased BET surface area, lack of complete dissolution of the MOF in Et_4NBr solution at room temperature and presence of both BPDC and Zn in the conversion mother liquor, as well as the uptake of Reichardt's dye post conversion and subsequent exclusion of larger diameter CdSe QDs all support the preferential dissolution of a single framework. Our studies, when taken in conjunction with existing literature,[21] suggest that the mechanism of deinterpenetration involves dissolution of a single framework with minimal effect on the remaining intact framework of the MOF *within the kinetic window of the reaction* (Figure 4). We propose that this process proceeds by initial attack of the halide on one of the frameworks at the Zn-node, leading to a Zn-halide intermediate.[11] Once this initial defect is introduced to one of the frameworks, it becomes kinetically favored to continue reacting (e.g. dissolving) over the intact framework. We speculate that initial halide attack may be assisted by defects already present in the framework due to potential partial interpenetration.[21]

In summary we have reported the deinterpenetration of IRMOF-9 by conversion *via* a putative dissolution mechanism. The structure of the product was confirmed *via* gas sorption analysis, PXRD, and size exclusion dye experiments.

Acknowledgements

There are no conflicts to declare. This research was funded by NSF Grant DMRRUI: 1807462 (J.L.S., C.J.T., D.T.G), the Donors of the American Chemical Society Petroleum Research Fund award #59835-DNI10 (A.B.C., J.I.F.), and the U.S. Department of Energy B.E.S. Grant No. DE-SC0004888 (C. A. C.).

Keywords: Metal–organic frameworks • Adsorption • Dyes/Pigments • Crystal engineering • Crystal growth • Microporous materials • IRMOF-9 • IRMOF-10 • Interpenetration

[1] a) B. F. Hoskins, R. Robson, *J. Am. Chem. Soc.* **1989**, *111*, 5962-5964; b) B. F. Hoskins, R. Robson, *J. Am. Chem. Soc.* **1990**, *112*, 1546-1554; c) S. Seth, A. J. Matzger, *Cryst. Growth Des.* **2017**, *17*, 4043-4048.

[2] a) H. Wang, J. Li, *Acc. Chem. Res.* **2019**, *52*, 1968-1978; b) Y. Wang, D. Zhao, *Cryst. Growth Des.* **2017**, *17*, 2291-2308; c) B. Li, H.-M. Wen, W. Zhou, B. Chen, *J. Phys. Chem. Lett.* **2014**, *5*, 3468-3479.

[3] a) C.-H. Wang, W.-Y. Gao, D. C. Powers, *J. Am. Chem. Soc.* **2019**, *141*, 19203-19207; b) A. H. Chughtai, N. Ahmad, H. A. Younus, A. Laypkov, F. Verpoort, *Chemical Society Reviews* **2015**, *44*, 6804-6849; c) M. Viciano-Chumillas, M. Mon, J. Ferrando-Soria, A. Corma, A. Leyva-Pérez, D. Armentano, E. Pardo, *Acc. Chem. Res.* **2020**, *53*, 520-531.

[4] a) Y. Wang, J. Yan, N. Wen, H. Xiong, S. Cai, Q. He, Y. Hu, D. Peng, Z. Liu, Y. Liu, *Biomaterials* **2020**, *230*, 119619; b) I. Abánades Lázaro, R. S. Forgan, *Coord. Chem. Rev.* **2019**, *380*, 230-259; c) L. Wang, M. Zheng, Z. Xie, *Journal of Materials Chemistry B* **2018**, *6*, 707-717.

[5] a) S. Rojas, P. Horcajada, *Chemical Reviews* **2020**, *120*, 8378-8415; b) S. Kuyuldar, D. T. Genna, C. Burda, *J. Mater. Chem. A* **2019**, *7*, 21545-21576; c) X. Li, B. Wang, Y. Cao, S. Zhao, H. Wang, X. Feng, J. Zhou, X. Ma, *ACS Sustainable Chemistry & Engineering* **2019**, *7*, 4548-4563; d) M. Ding, X. Cai, H.-L. Jiang, *Chem. Sci.* **2019**, *10*, 10209-10230.

[6] M. Eddaoudi, J. Kim, N. Rosi, D. Vodak, J. Wachter, M. O'Keeffe, O. M. Yaghi, *Science* **2002**, *295*, 469-472.

[7] B. F. Abrahams, B. F. Hoskins, D. M. Michail, R. Robson, *Nature* **1994**, *369*, 727-729.

[8] a) H.-L. Jiang, T. A. Makal, H.-C. Zhou, *Coord. Chem. Rev.* **2013**, *257*, 2232-2249; b) Y.-N. Gong, D.-C. Zhong, T.-B. Lu, *CrystEngComm* **2016**, *18*, 2596-2606; c) Q.-G. Zhai, X. Bu, X. Zhao, D.-S. Li, P. Feng, *Acc. Chem. Res.* **2017**, *50*, 407-417.

[9] T. A. Makal, A. A. Yakovenko, H.-C. Zhou, *J. Phys. Chem. Lett.* **2011**, *2*, 1682-1689.

[10] a) O. K. Farha, K. L. Mulfort, A. M. Thorsness, J. T. Hupp, *J. Am. Chem. Soc.* **2008**, *130*, 8598-8599; b) J. Zhang, L. Wojtas, R. W. Larsen, M. Eddaoudi, M. J. Zaworotko, *J. Am. Chem. Soc.* **2009**, *131*, 17040-17041.

[11] M. K. Bellas, J. J. Mihaly, M. Zeller, D. T. Genna, *Inorg. Chem.* **2017**, *56*, 950-955.

[12] a) J. L. C. Rowsell, O. M. Yaghi, *J. Am. Chem. Soc.* **2006**, *128*, 1304-1315; b) A. Khansari, M. R. Bryant, D. R. Jenkinson, G. B. Jameson, O. T. Qazvini, L. Liu, A. D. Burrows, S. G. Telfer, C. Richardson, *CrystEngComm* **2019**, *21*, 7498-7506; c) H. Khajavi, J. Gascon, J. M. Schins, L. D. A. Siebbeles, F. Kapteijn, *J. Phys. Chem. C* **2011**, *115*, 12487-12493; d) C. Wang, D. Liu, Z. Xie, W. Lin, *Inorg. Chem.* **2014**, *53*, 1331-1338; e) K. B. Sezginel, P. A. Asinger, H. Babaei, C. E. Wilmer, *Chem. Mater.* **2018**, *30*, 2281-2286; f) S. Canossa, L. Fornasari, N. Demitri, M. Mattarozzi, D. Choquesillo-Lazarte, P. Pelagatti, A. Bacchi, *CrystEngComm* **2019**, *21*, 827-834.

[13] R. Babarao, C. J. Coghlan, D. Rankine, W. M. Bloch, G. K. Gransbury, H. Sato, S. Kitagawa, C. J. Sumby, M. R. Hill, C. J. Doonan, *Chem. Commun.* **2014**, *50*, 3238-3241.

[14] S. Canossa, P. Pelagatti, A. Bacchi, *Isr. J. Chem.* **2018**, *58*, 1131-1137.

[15] a) S. Bureekaew, H. Sato, R. Matsuda, Y. Kubota, R. Hirose, J. Kim, K. Kato, M. Takata, S. Kitagawa, *Angewandte Chemie International Edition* **2010**, *49*, 7660-7664; b) M. Lange, M. Kobalz, J. Bergmann, D. Lässig, J. Lincke, J. Möllmer, A. Möller, J. Hofmann, H. Krautscheid, R. Staudt, R. Gläser, *J. Mater. Chem. A* **2014**, *2*, 8075-8085.

[16] J. I. Feldblyum, A. G. Wong-Foy, A. J. Matzger, *Chem. Commun.* **2012**, *48*, 9828-9830.

[17] K. Banlusan, E. Antillon, A. Strachan, *J. Phys. Chem. C* **2015**, *119*, 25845-25852.

[18] B. Liu, A. G. Wong-Foy, A. J. Matzger, *Chem. Commun.* **2013**, *49*, 1419-1421.

[19] L. Sarkisov, A. Harrison, *Molecular Simulation* **2011**, *37*, 1248-1257.

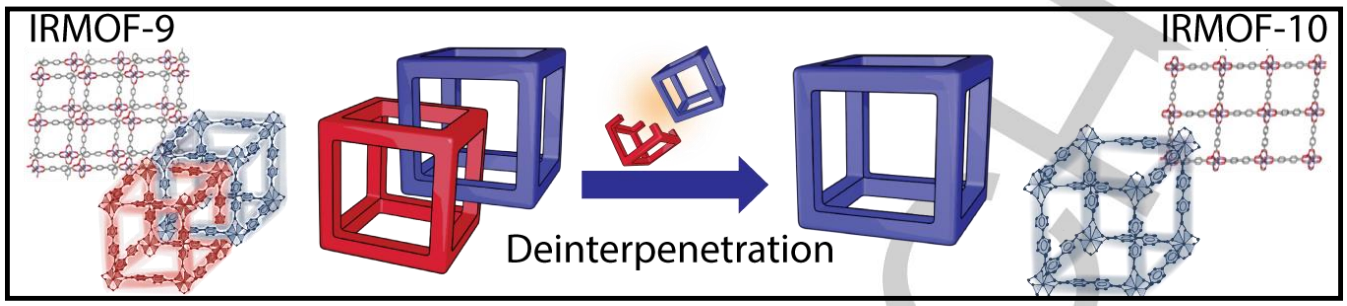
[20] M. L. Landry, T. E. Morrell, T. K. Karagounis, C.-H. Hsia, C.-Y. Wang, *J. Chem. Educ.* **2014**, *91*, 274-279.

[21] a) S. Yang, X. Lin, W. Lewis, M. Suyetin, E. Bichoutskaia, J. E. Parker, C. C. Tang, D. R. Allan, P. J. Rizkallah, P. Hubberstey, N. R. Champness, K. Mark Thomas, A. J. Blake, M. Schröder, *Nat. Mater.* **2012**, *11*, 710-716; b) G. Verma, S. Kumar, T. Pham, Z. Niu, L. Wojtas, J. A. Perman, Y.-S. Chen, S. Ma, *Cryst. Growth Des.* **2017**, *17*, 2711-2717; c) D. O'Nolan, D. G. Madden, A. Kumar, K.-J. Chen, T. Pham, K. A. Forrest, E. Patyk-Kazmierczak, Q.-Y. Yang, C. A. Murray, C. C. Tang, B. Space, M. J. Zaworotko, *Chem. Commun.* **2018**, *54*, 3488-3491; d) A. Ferguson, L. Liu, S. J. Tapperwijn, D. Perl, F.-X. Coudert, S. Van Cleuvenbergen, T. Verbiest, M. A. van der Veen, S. G. Telfer, *Nat. Chem.* **2016**, *8*, 250-257; e) D. Perl, S. J. Lee, A. Ferguson, G. B. Jameson, S. G. Telfer, *Nat. Chem.* **2023**.

This article is protected by copyright. All rights reserved

Author Manuscript

Entry for the Table of Contents



We report a new synthesis of deinterpenetrated IRMOF-9 (IRMOF-10) using a bromide-mediated deinterpenetration of IRMOF-9 *via* dissolution of the second interpenetrating network. A combination of gas sorption, X-ray diffraction, and dye exclusion tests corroborate the synthesis of a deinterpenetrated IRMOF-9 product.

Institute and/or researcher Twitter usernames: @GennaLab and @FeldblyumGroup

WILEY-VCH

Author Manuscript

This article is protected by copyright. All rights reserved